PAPER

All-fiber multimode interference micro-displacement sensor

Meas. Sci. Technol. **24** (2013) 055104 (7pp) doi:10.1088/0957-0233/24/5/055104

All-fiber multimode interference micro-displacement sensor

J E Antonio-Lopez[1], P LiKamWa[1,2], J J Sanchez-Mondragon[3] and D A May-Arrioja[4]

[1] CREOL, The College of Optics and Photonics, University of Central Florida, Orlando, FL 32816-2700, USA
[2] EECS Department, University of Central Florida, Orlando, FL 32816-2700, USA
[3] Instituto Nacional de Astrofísica, Óptica y Electrónica, A.P. 51 y 216, Tonantzintla, Puebla 72000, México
[4] Fiber and Integrated Optics Laboratory, Departamento de Ingeniería Electrónica, UAMRR, Universidad Autónoma de Tamaulipas, Reynosa, Tamaulipas 88779, México

E-mail: darrioja@uat.edu.mx

Received 3 January 2013, in final form 26 February 2013
Published 4 April 2013
Online at stacks.iop.org/MST/24/055104

Abstract
We report an all-fiber micro-displacement sensor based on multimode interference (MMI) effects. The micro-displacement sensor consists of a segment of No-Core multimode fiber (MMF) with one end spliced to a segment of single mode fiber (SMF) which acts as the input. The other end of the MMF and another SMF are inserted into a capillary ferrule filled with index matching liquid. Since the refractive index of the liquid is higher than that of the ferrule, a liquid MMF with a diameter of 125 μm is formed between the fibers inside the ferrule. When the fibers are separated this effectively increases the length of the MMF. Since the peak wavelength response of MMI devices is very sensitive to changes in the MMF's length, this can be used to detect micro-displacements. By measuring spectral changes we have obtained a sensing range of 3 mm with a sensitivity of 25 nm mm^{-1} and a resolution of 20 μm. The sensor can also be used to monitor small displacements by using a single wavelength to interrogate the transmission of the MMI device close to the resonance peak. Under this latter regime we were able to obtain a sensitivity of 7000 mV mm^{-1} and a sensing range of 100 μm, with a resolution up to 1 μm. The simplicity and versatility of the sensor make it very suitable for many diverse applications.

Keywords: sensors, MMI, multimode interference, multimode fiber, fiber sensor, micro-displacement

(Some figures may appear in colour only in the online journal)

1. Introduction

Nowadays, measurement of micro-displacements is very important not only for optical-based devices but also for some industrial applications where precise movement control is required such as bio-sensing, atomic force microscopy and micro-electro-mechanical systems. Depending on the application the equipment that is required for measuring micro-displacements may vary. Nevertheless, there is always the need for a system that is portable (low weight and size), has good sensitivity and that can be suitable for measurements to be made remotely. All-fiber-based optical micro-displacement sensors are very attractive due to their superior advantages over electronic systems, such as high sensitivity, immunity to electromagnetic interference and compact size. This kind of fiber sensor has been widely investigated since they offer high resolution, low cost, the possibility for multiplexing and light coupling is straightforward. Recently several kinds of fiber-based displacement sensors have been proposed and demonstrated. A micro-displacement sensor using a special two-core optical fiber (TCOF) was recently demonstrated [1]. In this configuration the TCOF is spliced between two

single mode fibers (SMF) in order to form a Mach–Zehnder interferometer. The TCOF is coiled into a small loop and micro-displacements on top of the loop provide a phase difference between the cores which is correlated into intensity variations. The main disadvantage for this sensor is that the cores have to be aligned and it has a rather small sensing range. Photonic crystal fibers (PCF) and fiber gratings, either fiber Bragg gratings or long period gratings, have also been used as displacement sensors [2–6]. However, in both cases, either the need for a PCF or having to engrave a grating might increase the final cost of the sensor. Different configurations have also been designed using multimode fibers (MMF). For example, a sensor using a MMF coupler was demonstrated, but the configuration was a little cumbersome and the resolution was only 70 μm depending on the light source employed [7]. A MMF bundle was also reported as a displacement sensor using an intensity modulation technique and a mirror as a reflecting target. However, the response is not linear for continuous sensing range and we have to separate two different sensing ranges in order to get a linear response [8]. The use of multimode interference (MMI) effects was recently demonstrated as a displacement sensor by placing a mirror in front of the MMF facet [11]. When the mirror is moved back and forth from the MMF facet, the displacement is recorded by monitoring the peak wavelength shift of the MMI response. The main drawback in this setup is that the mirror surface has to be exactly parallel to the MMF facet, which makes the alignment a complicated task and the overall response is very sensitive to vibrations. Additionally, the sensing range is limited to 200 μm due to high losses resulting from the free space propagation between the MMF facet and mirror.

Recently, the use of fiber-based MMI devices for filter or tunable laser applications has been demonstrated [12, 13]. The key advantages of MMI devices are that they exhibit a band-pass filter response and they only require splicing a MMF segment between two SMF segments. In this work we demonstrate a micro-displacement sensor based on MMI effects using a simple structure that eliminates alignment problems. The key component is a fused silica ferrule with an inner diameter of 125 μm. When this ferrule is filled with liquid we obtain a liquid multimode fiber (LMMF). In this way, when the separation between the MMF and SMF inside the ferrule is increased, the result is that the effective length of the MMF will be the sum of the solid MMF length plus the LMMF segment. This provides a stable and linear shift of the MMI response with minimum losses. This simple mechanism results in an MMI micro-displacement sensor with a sensing range of 3 mm, with a sensitivity of 25 nm mm^{-1} and a resolution of 20 μm, when the sensor is spectrally operated. This sensing range is 15 times better than the previous MMI sensor [11], and the sensitivity is 88 times better as compared to other reported spectral displacement sensors [2–4]. If the sensor is interrogated using a single wavelength (intensity operated), a sensing range of 100 μm with a sensitivity of 7000 mV mm^{-1} is obtained. This sensitivity is at least 40 times better than the highest sensitivity reported for the intensity operated micro-displacement sensor [8–10]. Based on our results, this configuration provides a simple, cost-effective, versatile and highly sensitive micro-displacement sensor.

2. Micro-displacement sensor principle and design

The MMI effect has been extensively studied on integrated devices to make different kinds of photonic devices for several applications [14]. The fundamental component in order to obtain MMI effects is to have a multimode waveguide (MMW) designed to support a large number of modes (typically $\geqslant$ 3). After the supported modes are excited by launching a field using a single mode waveguide (SMW) as the input, the interference between the modes propagating along the MMW gives rise to the formation of self-images of the input field along this MMW segment. The formation of such self-images occurs at periodic intervals, and depending on the transverse coupling position we can have the formation of single as well as multiple images. Therefore, the length of the MMW can be calculated in order to have a self-image right at the end of the MMW. If a SMW is placed where the self-image is formed all the light is coupled to this output SMW.

Since the only requirement to have the MMI effect is to have a MMW, we can also observe such MMI effects using optical fibers. A simple way to observe the basics behind the formation of MMI effects in optical fibers is to splice a SMF directly to a MMF segment with a step-index profile. Due to the circular symmetry of the fundamental mode of the SMF, the input light is assumed to have a field distribution of $\psi(r, \phi, 0)$, i.e. radial symmetry at $z = 0$. When the light is launched into the MMF, the input field can be decomposed into the guided modes of the MMF. Nevertheless, because of the radial symmetry of the SMF and assuming that the SMF axis is aligned with the MMF axis, only the LP_{0m} modes can be excited at $z = 0$ [15]. The input field can then be represented by

$$\psi(r, \phi, 0) = \sum_{\nu=1}^{m} c_\nu \varphi_\nu(r, \phi, 0), \tag{1}$$

where m is the number of guided modes, $\varphi_\nu(r, \phi, 0)$ is the νth guided mode of the MMF and c_ν is the mode expansion coefficient as estimated using an overlap integral:

$$c_\nu = \frac{\int\int \psi(r, \phi)\varphi_\nu(r, \phi)\, \mathrm{d}s}{\int\int |\varphi_\nu(r, \phi)|^2\, \mathrm{d}s}. \tag{2}$$

Neglecting mode conversion, all the excited modes propagate independently inside the MMF. Therefore, the field after propagating a distance z can be calculated by

$$\begin{aligned}\psi(r, \phi, z) &= \sum_{\nu=1}^{m} c_\nu \varphi_\nu(r, 0)\, \mathrm{e}^{-\mathrm{i}\beta_\nu z} \\ &= \mathrm{e}^{-\mathrm{i}\beta_1 z} \sum_{\nu=1}^{m} c_\nu \varphi_\nu(r, 0)\, \mathrm{e}^{-\mathrm{i}(\beta_\nu - \beta_1)z},\end{aligned} \tag{3}$$

where β_1 and β_ν are the propagation constants of the fundamental and the νth guided mode in the MMF. It is clear from equation (3) that when the phase factor $(\beta_\nu - \beta_1)z$ is an exact multiple of 2π we obtain an exact replica of the input field, and this is the distance where the MMF has to be cleaved to have a self-image right at the output MMF facet.

The process behind the formation of such self-images can be more easily observed by using a commercially available

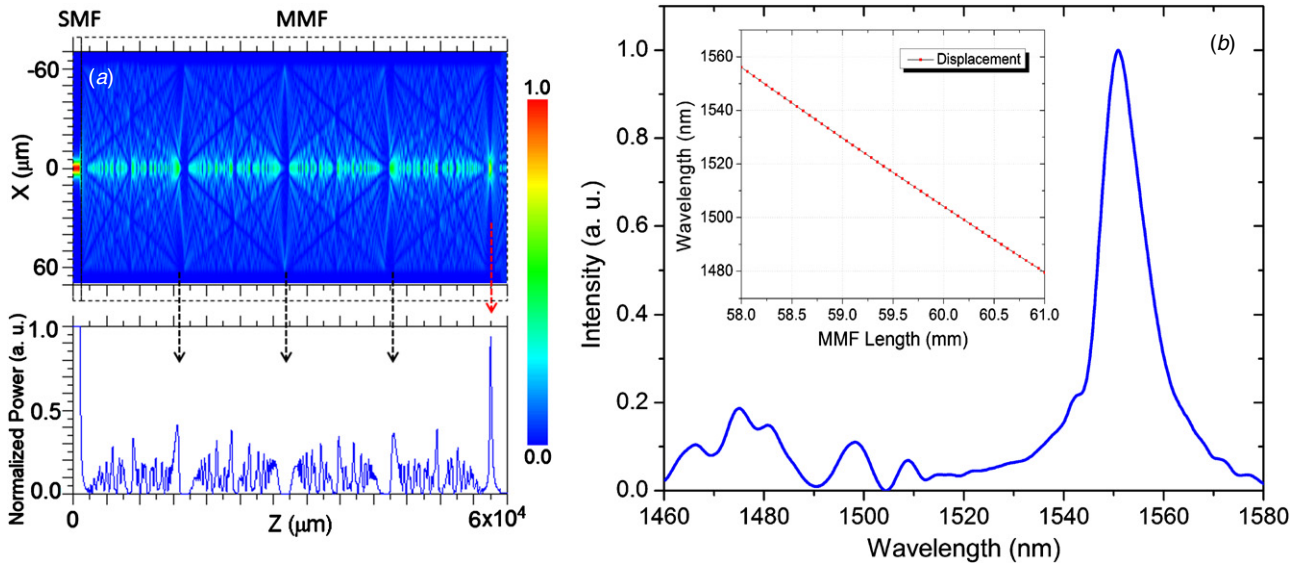

Figure 1. (*a*) Light propagation in an MMI fiber device at 1550 nm using only solid MMF and (*b*) spectral response of the MMI device (inset: peak wavelength response as a function of the MMF length).

beam propagation software package (BeamPROP from RSoft) as shown in figure 1(*a*). In this simulation, the input consists of a standard SMF (SMF-28) having a core diameter of 9 μm, with core and cladding refractive index (RI) of 1.4504 and 1.4447 at 1550 nm, respectively. The MMF has a core diameter of 125 μm and RI of 1.4440 at 1550 nm with air as the cladding. Light with a wavelength of 1550 nm is also used in the simulation. The positions of the images are marked by arrows with the image number increasing from left to right. As a result of the symmetric light coupling, beside the self-image (marked by the red arrow), we have the formation of pseudo-images (marked by the black arrows). Since these pseudo-images have more losses and their spectral bandwidth is broader we only operate the MMI at the real self-image (red arrow). As we pointed out previously, if we cleave the MMF exactly at the red arrow position and we splice an output SMF, only light with a wavelength of 1550 nm will be exactly imaged at this MMF–SMF output interface. Any other wavelength will form a self-image before or after this interface which will significantly reduce the light coupled to the output SMF. Therefore, when a continuum spectrum is sent through such a MMI device, a band-pass filter response is obtained as shown in figure 1(*b*).

Since MMI effects have been extensively investigated, a simple relationship can be obtained under the asymptotic formulation [16] by expressing the difference in the longitudinal propagation constants between two radial modes as a function of the MMF parameters (core RI and diameter) and the operating wavelength [17]. Therefore, by expressing the peak wavelength as a function of all other terms, we obtain the following expression:

$$\lambda_0 = \frac{4 n_{\mathrm{MMF}} D_{\mathrm{MMF}}^2}{L_{\mathrm{MMF}}}, \tag{4}$$

where λ_0 is the free space wavelength, n_{MMF} corresponds to the RI, D_{MMF} is the diameter and L_{MMF} is the length of the MMF. We can observe from equation (4) that the peak wavelength

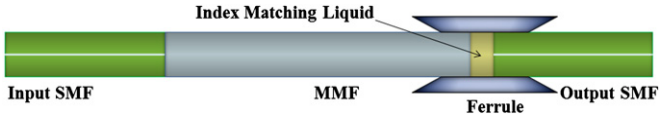

Figure 2. Schematic of the LMMI micro-displacement sensor.

is inversely proportional to the MMF length. Therefore, if the MMF length is increased, the peak wavelength will move to shorter wavelength values as shown in the inset of figure 1(*b*). The MMI response to variations in length is highly linear, which is good for sensing applications.

In order to exploit an MMI device as a micro-displacement sensor we propose the MMI configuration shown in figure 2. In this configuration a segment of MMF is spliced to a SMF, which acts as the input, while the other end of the MMF is cleaved to a specific length. This MMF end and another SMF are inserted into a fused silica ferrule. The ferrule has an inner diameter of 127 μm and is filled with an index matching liquid (Cargille®) whose RI value is higher than that of the ferrule, but lower than that of the MMF. Since the RI of the liquid is higher than that of the ferrule, a LMMF is formed between the fibers inside the ferrule. This allows us to separate the MMF and SMF ends inside the ferrule and effectively increases the total MMF length, which is now the sum of the MMF and the LMMF. According to equation (4) this increment should be reflected as a linear peak wavelength shift. Therefore, micro-displacements will be recorded as a peak wavelength shift of the MMI spectral response. A beam propagation analysis of the MMF–LMMF structure shown in figure 2 was also performed to study the effects of the liquid section on the light propagation. Here we replaced 3 mm of the MMF by a LMMF formed by liquid and ferrule with RI of 1.442 and 1.440, respectively. As shown in figure 3(*a*), the interference carpet does not exhibit any detrimental effects due to the MMF–LMMF interface, and the self-image appears to be formed at the same longitudinal position. A closer inspection reveals a

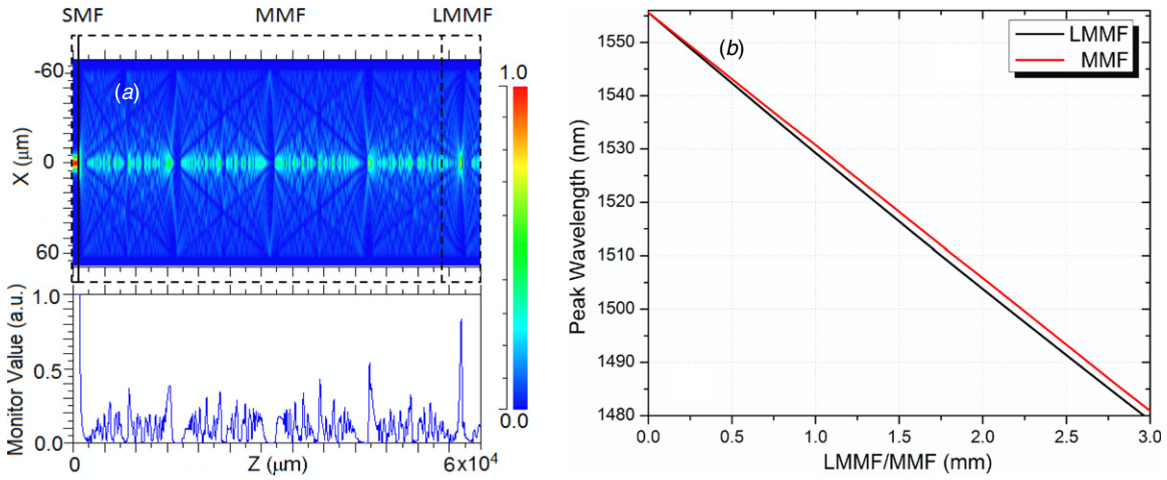

Figure 3. (*a*) Light propagation in a LMMI fiber device at 1550 nm in which 3 mm of solid MMF has been replaced by LMMF and (*b*) peak wavelength response of the LMMI and MMI as a function of the LMMF and MMF, respectively.

minimal change of the original position of the self-image due to the liquid. From now on, the structure shown in figure 2 will be referenced as a liquid MMI (LMMI) device.

In order to obtain the exact peak wavelength response of the LMMI as a function of the LMMF length, equation (4) has to be modified to include the phase contribution of each kind of fiber that is forming the LMMI, i.e. the MMF and the LMMF [18]. Therefore, the peak wavelength in this case is calculated by

$$\lambda_0 = \frac{4n_{\mathrm{LMMF}}D^2_{\mathrm{LMMF}}}{L_T}\left(\frac{L_{\mathrm{LMMF}}}{L_T}\right) + \frac{4n_{\mathrm{MMF}}D^2_{\mathrm{MMF}}}{L_T}\left(\frac{L_{\mathrm{MMF}}}{L_T}\right), \tag{5}$$

where n_{LMMF} corresponds to the RI, D_{LMMF} is the diameter and L_{LMMF} is the length of the LMMF. L_T is the total fiber length including both the MMF and the LMMF. The variables in the second term of equation (5) are the same as described in equation (4) for the solid MMF. Using equation (5) we can plot the peak wavelength response of the LMMI sensor as a function of the LMMF increment (i.e. displacement). As shown in figure 3(*b*), the response is highly linear since we are only modifying the lengths of the LMMF and the total fiber length (L_T). As a comparison, we also plot the response of an MMI device when the solid MMF is incremented by similar values. We can notice a small difference in the slope of the response, which is related to the LMMF which has a slightly different effective RI and diameter than that of the solid MMF. Our configuration allows larger separations between the fibers because the LMMF keeps the light confined. This is of course correlated with a huge enhancement in the measurable micro-displacement range with minimum losses. The advantage of our sensor is that the peak wavelength can be easily selected by changing the length of the MMF section. This also allows for a simple way to achieve multiplexed operation.

3. Experimental setup

The response of the MMI micro-displacement sensor is characterized using the setup shown in figure 4. Light from

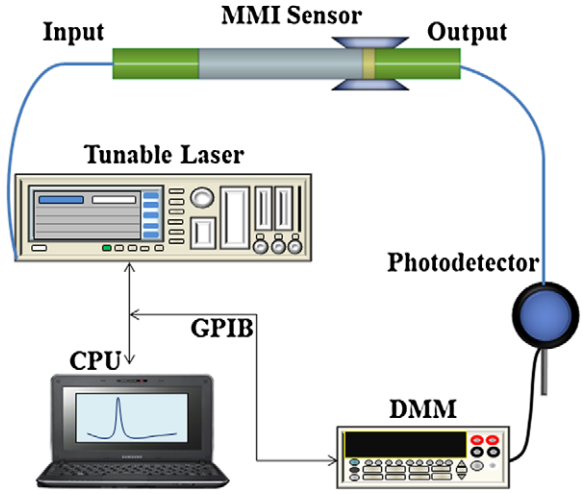

Figure 4. Experimental setup for MMI micro-displacement sensor characterization.

an Agilent tunable laser (1460 to 1580 nm) is coupled into the input SMF, and the light transmitted through the MMI sensor is collected through the SMF output. The transmitted light is measured using an InGaAs photodetector which is connected to a Keithley digital multimeter (DMM), and the setup is fully controlled through GPIB ports using LabVIEW. Each SMF is held in place using two *XYZ* translation stages which set the starting position, while also allowing longitudinal movement of one of the fibers with micrometer resolution. The fused silica ferrule has a total length of 15 mm, and an inner and outer diameter of 127 μm and 17.5 mm, respectively (Polymicro Technologies). The ends of the ferrule are flared to facilitate the fiber insertion into the capillary. Regarding the MMF, it is very important to mention that any kind of step-index MMF can be used to observe MMI effects. However, the MMF used in our experiments is a specialty fiber known as No-Core fiber, which has a core RI of 1.444 at 1550 nm with air as its cladding. This provides a MMF with a core diameter of 125 μm, which allows a smooth transition from the solid MMF to the LMMF. This fiber was selected since having a bigger RI difference between the core and cladding

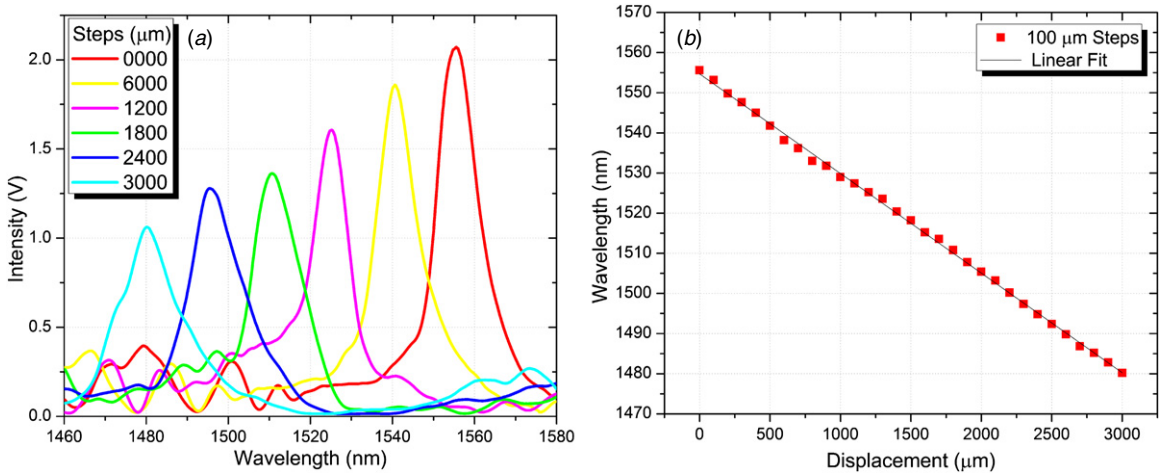

Figure 5. (*a*) Spectral response and (*b*) peak wavelength response of the LMMI micro-displacement sensor as a function of the separation between fibers inside the ferrule.

provides a narrower MMI band-pass filter bandwidth, as well as a higher contrast. The length of the No-Core fiber was 58.016 mm, which corresponds to the fourth self-image at a peak wavelength of 1555.6 nm. This self-image number is selected because it exhibits the lowest insertion loss and also the narrowest wavelength bandwidth as compared to the other lower order self-images. Given the ferrule inner diameter and No-Core fiber diameter, the fibers are reasonably aligned in the transverse direction after their insertion into the ferrule. This allows us to move the fiber smoothly along the propagation direction by moving the micrometer of the translation stage, which provides the ability to control micro-displacements as small as 10 μm.

4. Results and discussions

The micro-displacement sensor performance is characterized by increasing the separation between the SMF and MMF in small steps and measuring its spectral response at each step. The spectral response is acquired by tuning the wavelength of the laser while maintaining constant power at every wavelength.

As shown in figure 5(*a*), when the fibers are in contact with each other a nice band-pass filter response is obtained with a peak wavelength of 1555.6 nm. As we increase the separation between the fibers inside the ferrule, the LMMF formed in the ferrule increases the total fiber length of the LMMI and the micro-displacement should be detected as a peak wavelength shift. As expected, the LMMI peak wavelength experiences a blue-shift of 15 nm for every 600 μm increment in the separation of the fibers as shown in figure 5(*a*). However, we also notice that as the separation between the fiber facets is increased, the insertion losses are also increased to a value of almost 3 dB for a maximum separation of 3000 μm. We believe that this is related to the small diameter mismatch between the diameter of the silica ferrule (127 μm) and that of the No-Core and SMF fibers (125 μm), as well as ferrule inner wall imperfections. Therefore, as the fibers move away from each other there is the possibility of some tilting between the facets which can deteriorate the coupling of the self-image to the output SMF. As a result, we limit the displacement or sensing range (i.e. maximum gap between fiber facets) to 3000 μm, just before the insertion loss falls below 3 dB. After setting this maximum range, one of the fibers can be moved back and forth from the starting up to the maximum position. If higher losses can be tolerated the sensor can be operated up to a maximum range of 4000 μm. Therefore, a more uniform capillary with a diameter closer to the standard 125 μm diameter of the fibers should in principle allow us to increase our displacement range with the insertion loss as low as possible.

The behavior of the LMMI peak wavelength against micro-displacements is shown in figure 5(*b*), where the sensor response was acquired for steps of 100 μm. The response of the sensor is not only very linear, which is a plus for a sensor, but the maximum wavelength shift corresponds very closely to the calculated value for a displacement of 3 mm. This provides a sensitivity of 25 nm mm^{-1} for our LMMI sensor, which is 88 times better as compared to other reported spectral micro-displacement sensors. The highest resolution that can be obtained, and still be able to resolve the LMMI peak wavelength shift, was measured at 20 μm as shown in figure 6(*a*). We could push for higher resolution, but resolving the MMI peak becomes difficult due to the bandwidth of the sensor response. An even higher resolution can be easily achieved by measuring the intensity changes as a function of the micro-displacement, but interrogating the LMMI with a single wavelength. As we can see in figure 5(*a*) the spectra shift to shorter wavelengths, and this allows us to interrogate the LMMI sensor using either one of the slopes adjacent to the LMMI peak. In our case we interrogated the LMMI sensor at a wavelength of 1550 nm, and the results are shown in figure 6(*b*). Micro-displacement steps of 20 and 10 μm are easily resolved this way, and this minimum increment was limited by our available micrometer. Based on our results, we believe that a resolution up to 1 μm is feasible. The sensitivity in this case is 7000 mV mm^{-1}, with a sensing range up to 100 μm.

Since the sensor operates based on the spectral shift of the LMMI response, temperature effects need to be taken into

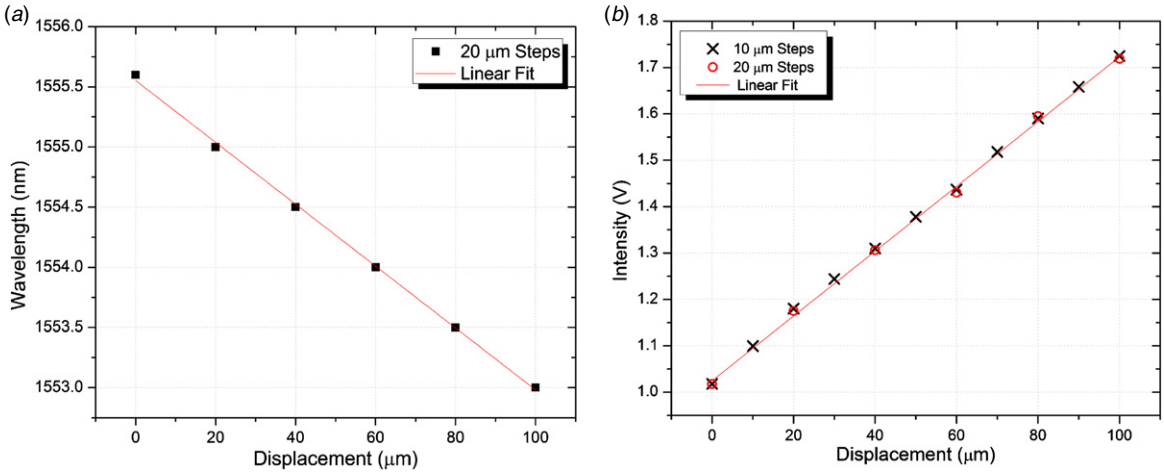

Figure 6. (*a*) Peak wavelength response and (*b*) intensity response of the sensor as a function of the micro-displacement with different steps.

account. Considering that Cargille liquids cannot be reliably operated beyond 100 °C, we measured the MMI and LMMI spectral shift as a function of temperature from 25 to 100 °C. In a standard MMI device, using only No-Core fiber, we observe a spectral red-shift of 0.9415 nm which corresponds to a sensitivity of 0.0125 nm °C^{-1}. In our LMMI device, the liquid section should make the device more sensitive to temperature because it has a thermo-optic coefficient (TOC) of $\Delta n/\Delta T = -3.9 \times 10^{-4}$ °C^{-1} which is two orders of magnitude higher as compared to silica ($\Delta n/\Delta T = 7 \times 10^{-6}$ °C^{-1}). However, the TOC of the liquid has the opposite sign which could compensate the thermal effects from the silica section. We should highlight that in order to make such measurements the RI of the liquid has to be increased because at higher temperatures the RI is reduced, and we need to keep its RI higher than that of the ferrule. We selected a RI of 1.475 which is reduced to 1.4458 at 100 °C. We should also note that even when at room temperature the liquid RI is higher than that of the No-Core fiber; the losses were not significantly increased due to the small section of liquid covering the No-Core fiber at the end of the ferrule. Measurements were carried out with the 3 mm long liquid section and as the temperature is increased the LMMI shows a maximum blue-shift of −0.6130 nm at 100 °C, which corresponds to a sensitivity of −0.0081 nm °C^{-1}. It is clear that the liquid section provides a stronger thermal response since it changes the slope of the temperature response, but the final result is that the absolute wavelength shift is reduced. Although this absolute wavelength shift is small, and should be even smaller when the length of the liquid section is reduced, temperature stabilization is required to obtain consistent micro-displacement measurements.

As compared to other structures our LMMI sensor has several advantages. Given the filtering nature of the sensor, multiplexed measurements can be achieved by just using different solid MMF lengths which provide a different initial peak wavelength at 0 μm displacement. The sensor is also assembled by cleaving and splicing fiber which makes it very simple to fabricate. We can use it either in transmission, as demonstrated here, or in reflection, using a section of SMF with a gold mirror on the facet outside the ferrule, and an optical circulator. Based on its operation regime (spectral or intensity) we can have a wide sensing range with a resolution up to 20 μm, as well as very high resolution (feasible up to 1 μm) with a sensing range of 100 μm. We consider that these advantages provide a highly desirable sensor that can find application in many different fields.

5. Conclusions

We have proposed and demonstrated a simple and effective fiber optic micro-displacement sensor based on MMI effects. The principle of the sensor relies on a capillary ferrule filled with index matching liquid to form a LMMF. This simple device allows us to effectively increase the length of the MMF segment in an MMI device. Since the peak wavelength response of MMI devices is very sensitive when the MMF length is modified, this can be used to detect micro-displacements. Using this LMMI sensor a sensing range of 3 mm, with a sensitivity of 25 nm mm^{-1} and a resolution of 20 μm, is observed when we measure the spectral response of the sensor. The sensor can also be intensity operated by interrogating the MMI with a single wavelength tuned to one of the slopes of the MMI response. Under this regime we obtain a sensitivity of 7000 mV mm^{-1} and a sensing range of 100 μm, with a resolution up to 1 μm. The simplicity and versatility of the sensor make it very suitable for different applications.

Acknowledgments

This work was supported by the Consejo Nacional de Ciencia y Tecnología (CONACyT) under contracts CB-2010/157866 and CB-2008/101378.

References

[1] Serpa C M, Torres P and Margulis W 2006 Micro-displacement sensor using a curved two-core optical fiber *OSA/Opt. Fiber Sens. OFS* p ThE37

[2] Jiang Q and Hu D 2011 Microdisplacement sensor based on tilted fiber Bragg grating transversal load effect *IEEE Sensors J.* **11** 1776–9

[3] Zhang H, Liu B, Wang Z, Luo J, Wang S, Jia C and Ma X 2010 Temperature-insensitive displacement sensor based on high-birefringence photonic crystal fiber loop mirror *Opt. Appl.* **40** 209–17
[4] Guo T, Chen C and Albert J 2009 Non-uniform-tilt-modulated fiber Bragg grating for temperature-immune micro-displacement measurement *Meas. Sci. Technol.* **20** 034007
[5] Chuang K C and Ma C C 2008 Pointwise fiber Bragg grating displacement sensor system for dynamic measurements *Appl. Opt.* **47** 3561–7
[6] Das K K and Alam M S 2002 Fiber-optic microdisplacement sensor based on diffraction grating *Microw. Opt. Technol. Lett.* **32** 446–9
[7] Yasin M, Harun S W, Samian K and Ahmad H 2009 Simple design of optical fiber displacement sensor using a multimode fiber coupler *Laser Phys.* **19** 1446–9
[8] Yasin M, Harun S W, Karyono K and Ahmad H 2008 Fiber-optic displacement sensor using a multimode bundle fiber *Microw. Opt. Technol. Lett.* **50** 661–3
[9] Trudel V and St-Amant Y 2009 One-dimensional single-mode fiber-optic displacement sensor for submillimeter measurements *Appl. Opt.* **48** 4851–7
[10] Miclos S and Zisu T 2001 Chalcogenide fiber displacement sensor *J. Optoelectron. Adv. Mater.* **3** 373–6
[11] Mehta A, Mohammed W S and Johnson E 2003 Multimode interference-based fiber-optic displacement sensor *IEEE Photonics Technol. Lett.* **15** 1129–31
[12] Mohammed W S, Smith P W E and Gu X 2006 All-fiber multimode interference bandpass filter *Opt. Lett.* **31** 2547–9
[13] Selvas R, Torres-Gomez I, Martinez-Rios A, Alvarez-Chavez J, May-Arrioja D A, LiKamWa P, Mehta A and Johnson E 2005 Wavelength tuning of fiber laser using multimode interference effects *Opt. Express* **13** 9439–45
[14] Soldano L B and Pennings E C M 1995 Optical multi-mode interference devices based on self-imaging: principles and applications *J. Lightwave Technol.* **13** 615–27
[15] Shalaby B M, Kermene V, Pagnoux D and Barthelemy A 2008 Transverse mode control by a self-imaging process in a multimode fibre laser using a single-mode feedback loop *J. Opt. A: Pure Appl. Opt.* **10** 115303
[16] Marcuse D 1987 Mode conversion in optical fibers with monotonically increasing core radius *J. Lightwave Technol.* **5** 125–33
[17] Mohammed W S, Mehta A and Johnson E G 2004 Wavelength tunable fiber lens based on multimode interference *J. Lightwave Technol.* **22** 469–77
[18] Antonio-Lopez J E, Sanchez-Mondragon J J, LiKamWa P and May-Arrioja D A 2010 Fiber-optic sensor for liquid level measurement *Opt. Lett.* **36** 3425–7